

Virtual Torque and Power Control of a Three-Phase Converter Connected to an Unbalanced Grid with Consideration of Converter Current Constraint and Operation Mode

Grzegorz Iwanski, *Member, IEEE*,

Abstract—The paper presents three-phase power converter control under grid voltage imbalance. The proposed method adapts the current imbalance in relation to the inverter or rectifier operation. Under the inverter operation, the control target is to have the non-oscillatory p component of instantaneous power and the x_r component of instantaneous virtual torque calculated as the dot product of the grid virtual flux vector and the converter current vector. Then, the phase with lower voltage is supported by higher current. In the rectifier mode, the control target is to have the non-oscillatory q component of power and the T_r component of virtual torque calculated as the cross product of the virtual flux and the converter current. This way, the phase with the highest voltage is loaded by higher current. Unbalanced current obtained in both targets is limited in the way that allows to limit true phase current and retain sinusoidal current waveforms. However, it does not allow maximum power transfer at the given grid voltage asymmetry, so in order to increase the power value, current progressive balancing is proposed in both operation modes. Finally, converter current balancing is applied also in the case in which a significant amount of reactive power is referenced.

Index Terms—AC-DC power conversion, current control, current limiters, power control, torque control.

I. INTRODUCTION

UNBALANCED grid operation of three-phase power converters during asymmetrical voltage sags has recently become an important research issue. Classic methods like vector control [1][2], or direct power control DPC [3][4] are sensitive to transformation angle distortions, which if calculated without filtration, introduce current waveforms deterioration in the case of grid voltage distortions.

In order to keep sinusoidal current under grid voltage harmonics, the phase locked loop PLL or virtual flux orientation [5][6] are introduced to remove oscillations from the transformation angle. Although both methods of reference frame angle filtration have similar properties in case of harmonics distorted grid, the PLL has an advantage over classic virtual flux orientation in the case of unbalanced voltage. The virtual flux orientation reduces transformation angle oscillations caused by grid voltage harmonics, but it does not reduce oscillations caused by grid voltage asymmetry, because the content of positive and negative sequence in the virtual flux is the same as in grid voltage. To avoid transformation, the converter current can be controlled in the stationary $\alpha\beta$ frame with proportional-resonant PR controllers. However, even in this case the reference signals must be assigned properly to achieve the targets of converter current during unbalanced grid conditions.

Power converter structure allowing both inverter and rectifier modes of operation for unbalanced grid voltage is presented in Fig. 1. The i_{dc} current will be created in the laboratory unit by the second three-phase converter fed from a separate grid and controlled by classic voltage oriented vector control method in a dq frame.

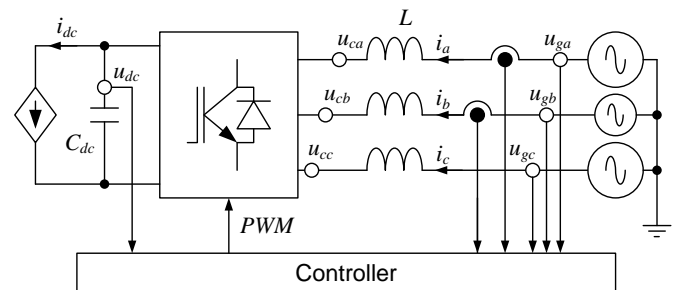


Fig. 1. Scheme of three-phase power converter connected to an unbalanced grid.

The Work is supported by National Science Centre within the Project granted on the basis of the decision number 2016/23/B/ST7/03942.

Author is with the Institute of Control and Industrial Electronics, Warsaw University of Technology, 00-662 Warszawa, Poland (corresponding author contact phone: +4822 2347415; fax: +4822 2346023; e-mail: iwanskig@isep.pw.edu.pl)

The possible targets are symmetrical current [7]-[9], current asymmetry opposite to voltage asymmetry (constant p component of instantaneous power) [10][11], and current asymmetry corresponding to voltage asymmetry (constant q component of instantaneous power) [12]-[19]. The constant p power component target providing sinusoidal current with imbalance opposite to voltage imbalance is beneficial in the inverter operation mode, because the phase with lower voltage is supported by higher current. It does not produce DC voltage oscillations that occur in the other targets. The constant q power component produces current imbalance corresponding to grid voltage imbalance, which means a unity power factor in each phase. This target does not deepen voltage asymmetry in the rectifier mode, because the phase with higher voltage is loaded more than the other phases. A thorough analysis of power inverter operation in a distribution grid under unbalanced voltage has been made in [20].

Although different targets of power/current are analyzed in a number of papers in detail, and their positive or negative influence on the converter operation and grid voltage conditions are described, a criteria and, in consequence, algorithms for targets change are rarely discussed. The authors of [21] propose progressive change of the target from the constant p component of power to symmetrical current target (progressive current balancing) in order to avoid exceeding the maximum current. The paper presents a detailed analysis confirmed by wide laboratory tests results including transients. However, the current limitation is set so that the maximum vector length does not exceed the radius of the circular hodograph representing the maximum sinusoidal balanced current. This can be equal to the phase current limitation only in the case in which the major semi-axis of the elliptical hodograph lies along one of the phase axes. In other cases, the elliptic hodograph does not touch the hexagon and the maximum phase current is not reached until it is fully balanced.

The targets change for converter current has been achieved also in [22]. Although the targets change has been well explained, the criteria for targets change have not been provided, and the target is selected and progressively changed in an arbitrary way by introduction of factors k_p , k_q , responsible for the content of negative sequence active and reactive current without taking into consideration converter current constraints. The paper presents a four-leg converter able to eliminate the zero sequence component in the four-wire system. However, the goal of zero sequence current elimination can be naturally achieved in the three-wire system topology, where the zero sequence cannot flow, so the application of a four-wire system in such a case is questionable. The control method presented in the cited paper does not have a deeper justification (cascaded control of grid side inductance current and converter side inductance current

of an LCL filter). The inner control structure has not been the main point of the paper, but it should allow, at least in the steady state, a satisfactory quality of the generated current, but it does not. Experimental results are not satisfactory due to poor current quality. An interesting point of the paper is introduction of a factor that allows flexible targets change and to reach intermediary steady states between the targets. However, the DC voltage oscillations should not necessarily be the main criteria of factor assignment in most cases, but the phase currents constraints and operation mode (inverter or rectifier) should. The issue of current limitation has not been analyzed in the paper.

[23] shows the progressive balancing method for a three-phase converter using instantaneous virtual grid torque calculation for rectifier operation taking into account the unbalanced phase current true limitation, and some comparison between the current limitation methods. Progressive balancing has been achieved through the introduction of intermediate $\alpha\beta$ to dq transformation and reduction of 100Hz current vector components oscillations in this frame using band pass filters with an adaptive damping factor. The paper was related only to rectifier operation so the constant p power component target (current asymmetry opposite to voltage asymmetry) was not implemented. In the current paper, the instantaneous virtual torque control method was mixed with the instantaneous power control method to achieve the required targets for both the rectifier mode and the inverter mode. This way the current balancing structure has been obtained in a simpler manner without intermediate $\alpha\beta$ to dq transformation and adaptive band pass filters, but with weighting factors providing weighted equivalent asymmetry of the current in the range of asymmetries between corresponding and opposite asymmetry of voltage. Additionally, the true phase current limitation method has been simplified by elimination of phase locked loops in these structures.

II. CONVERTER REFERENCE CURRENT CALCULATION

A. Instantaneous orthogonal torque components assignment

Equations (1)(2) describe a grid connected active rectifier equipped with an inductive filter, in the $\alpha\beta$ frame.

$$u_{c\alpha} = -R_L i_\alpha - L \frac{di_\alpha}{dt} + u_{g\alpha} \quad (1)$$

$$u_{c\beta} = -R_L i_\beta - L \frac{di_\beta}{dt} + u_{g\beta} \quad (2)$$

u_g is the grid voltage vector, i is the current vector, u_c is the voltage vector created by the power converter, R_L is the inductor resistance, and L is the filter inductance.

The DC voltage derivative (3) depends on the p component of instantaneous power and load current i_{dc} .

$$\frac{du_{dc}}{dt} = \frac{1}{C_{dc}} \left(\frac{p}{u_{dc}} - i_{dc} \right) \quad (3)$$

The p and q component of instantaneous power by Akagi is calculated by (4)(5)

$$p = \frac{3}{2} (u_{g\alpha} i_\alpha + u_{g\beta} i_\beta) \quad (4)$$

$$q = \frac{3}{2} (u_{g\beta} i_\alpha - u_{g\alpha} i_\beta) \quad (5)$$

Analogously to the power components equations, equations describing the virtual torque orthogonal components T_v , and x_v (6)(7) can be introduced. It has to be noted that the torque components are calculated in the manner in which the positive sign of T_v is for rectifier operation and the positive sign of x_v is for inductive reactive power.

$$T_v = \frac{3}{2} (\psi_{g\alpha} i_\beta - \psi_{g\beta} i_\alpha) \quad (6)$$

$$x_v = \frac{3}{2} (\psi_{g\alpha} i_\alpha + \psi_{g\beta} i_\beta) \quad (7)$$

i_α , i_β are converter current vector components in $\alpha\beta$ coordinates, $\psi_{g\alpha}$, $\psi_{g\beta}$ – virtual flux vector components.

These new variables can help to assign the reference current for the targets allowing asymmetrical current in both inverter and rectifier modes, respectively. The DC link controller references the p component of power according to (3) and the q component of power is referenced arbitrarily (or optionally from a superior algorithm, depending on the grid code). It is possible to assign reference instantaneous virtual torque components T_v , x_v , as a function of pq power components.

Based on equations (6)(7), and replacement of the actual variables with the reference ones, the current vector components can be derived as a function of the pq component of instantaneous power (8)(9).

$$i_\alpha = \frac{2}{3} \left(\frac{u_{g\alpha}}{u_{g\alpha}^2 + u_{g\beta}^2} p + \frac{u_{g\beta}}{u_{g\alpha}^2 + u_{g\beta}^2} q \right) \quad (8)$$

$$i_\beta = \frac{2}{3} \left(\frac{u_{g\beta}}{u_{g\alpha}^2 + u_{g\beta}^2} p - \frac{u_{g\alpha}}{u_{g\alpha}^2 + u_{g\beta}^2} q \right) \quad (9)$$

Based on (6)-(9), the torque components can be assigned as a function of power components (10)(11).

$$T_v = \frac{(\psi_{g\alpha} u_{g\beta} - \psi_{g\beta} u_{g\alpha})}{u_{g\alpha}^2 + u_{g\beta}^2} p + \frac{-(\psi_{g\alpha} u_{g\alpha} + \psi_{g\beta} u_{g\beta})}{u_{g\alpha}^2 + u_{g\beta}^2} q = k_{11} p + k_{12} q \quad (10)$$

$$x_v = \frac{(\psi_{g\alpha} u_{g\alpha} + \psi_{g\beta} u_{g\beta})}{u_{g\alpha}^2 + u_{g\beta}^2} p + \frac{(\psi_{g\alpha} u_{g\beta} - \psi_{g\beta} u_{g\alpha})}{u_{g\alpha}^2 + u_{g\beta}^2} q = k_{21} p + k_{22} q \quad (11)$$

Instantaneous values of factors k_{11} - k_{22} are oscillating during the grid voltage period, but their average values can be identified as (12)(13).

$$avg(k_{11}) = avg(k_{22}) = \omega_s^{-1} \quad (12)$$

$$avg(k_{12}) = avg(k_{21}) = 0 \quad (13)$$

Although the assumptions (14)(15) are mathematically not accurate, because the product of average values is not equal to the average value of the product, the existing error concerns the internal control variables p , q , T_v , x_v .

$$avg(T_v) = \omega_s^{-1} p + 0q = \omega_s^{-1} p \quad (14)$$

$$avg(x_v) = 0p + \omega_s^{-1} q = \omega_s^{-1} q \quad (15)$$

The true average values of virtual torque components T_v and x_v can be calculated using low pass filters of the terms $k_{11}p$ and $k_{12}q$, $k_{21}p$ and $k_{22}q$ (10)(11), but introduction of additional low pass filters will deteriorate control dynamics. The variables are referenced directly from outer controllers and these outer controllers will compensate for the occurring error.

B. Calculation of the reference current based on reference virtual torque and instantaneous power components

Two sets of reference variables are used for reference converter current calculation. For the target giving the same asymmetry of current as asymmetry of voltage, which is beneficial for the grid in the rectifier mode, the p component of power is of oscillatory character. Determination of adequate oscillations of p power components requires a number of calculations and signals decomposition in classic methods. However, the relation in a DFIG system [24] has been found that for this target the electromagnetic torque is constant and can be used as a reference. Due to the similarity, the calculated virtual torque component T_v and the q component of instantaneous power (5)(6), which are fixed in this target, can be used for reference current components calculation (16)(17).

$$i_{\alpha 1}^* = \frac{2}{3} \left(\frac{u_{g\alpha}}{\psi_{g\alpha} u_{g\beta} - \psi_{g\beta} u_{g\alpha}} T_v^* + \frac{\psi_{g\alpha}}{\psi_{g\alpha} u_{g\beta} - \psi_{g\beta} u_{g\alpha}} q^* \right) \quad (16)$$

$$i_{\beta 1}^* = \frac{2}{3} \left(\frac{u_{g\beta}}{\psi_{g\alpha} u_{g\beta} - \psi_{g\beta} u_{g\alpha}} T_v^* + \frac{\psi_{g\beta}}{\psi_{g\alpha} u_{g\beta} - \psi_{g\beta} u_{g\alpha}} q^* \right) \quad (17)$$

For the second target giving current asymmetry opposite to voltage asymmetry, which is beneficial for the grid during the inverter mode, the p component of power is constant, but the q component is of oscillatory character. The required oscillations of the q power component have to be determined to assign the correct value of reference current. However, instead of q power component assignment, the x_v^* component of virtual torque can be used for reference current components $i_{\alpha 2}^*$, $i_{\beta 2}^*$ calculation (18)(19)

$$i_{\alpha 2}^* = \frac{2}{3} \left(-\frac{\psi_{g\beta}}{\psi_{g\alpha} u_{g\beta} - \psi_{g\beta} u_{g\alpha}} p^* + \frac{u_{g\beta}}{\psi_{g\alpha} u_{g\beta} - \psi_{g\beta} u_{g\alpha}} x_v^* \right) \quad (18)$$

$$i_{\beta 2}^* = \frac{2}{3} \left(\frac{\psi_{g\alpha}}{\psi_{g\alpha} u_{g\beta} - \psi_{g\beta} u_{g\alpha}} p^* - \frac{u_{g\alpha}}{\psi_{g\alpha} u_{g\beta} - \psi_{g\beta} u_{g\alpha}} x_v^* \right) \quad (19)$$

This way, using the sets of reference variables p^* - x_v^* , and T_v^* - q^* , the reference currents for both targets are calculated. A detailed scheme of the method is presented in Fig. 14. Reference p^* power signal is produced by a DC voltage controller, whereas the q^* component of power is provided by an arbitrary signal q^{ref} and some correction signal q_{corr} . Correction signal q_{corr} produced by a power controller is introduced due to the fact that in the case of x_v^* control, the average value q_{avg} of the power component is different from arbitrarily referenced signal q^{ref} . Similarly in the case in which the T_v^* component of torque is used for reference current calculation, the reference p^* component of power is not equal to its average value during unbalanced grid connection. This is

caused by simplifications of (14)(15). However, the DC voltage controller and the introduced q power component correction controller eliminate steady state errors resulting from the mentioned simplifications.

Although there are several theories related to reactive power and different methods of its calculation, other signals than the average value of the q power component (by Akagi (5)) can be used as reactive power indicators. However, this may change only the input part related to actual reactive power calculation and the rest of control is left without modifications. An exemplary way of another reactive power calculation is the use of the dot product of the grid voltage vector delayed by $\pi/2$, and the converter current vector [17]. Calculated this way the q_{\perp} component of power (20) is equivalent to the x_v component scaled by grid voltage pulsation ω_s (20).

$$q_{\perp} = \frac{3}{2} (u_{g\alpha}^d i_{\alpha} + u_{g\beta}^d i_{\beta}) = \omega_s x_v \quad (20)$$

the $u_{g\alpha}^d$, $u_{g\beta}^d$ are grid voltage vector components in $\alpha\beta$ coordinates delayed by $\pi/2$, that means by 5ms for 50Hz.

However, neither the instantaneous values of q and q_{\perp} nor their average values q_{avg} and $q_{\perp avg}$ are equal so the correction controller of average q power is introduced to obtain exact value of q_{avg} power at reference level. Using the average values of the classic Akagi's p component of power (4) and the q_{\perp} component of power (20) as primary reference signals, the reference current vector components $i_{\alpha pq\perp}^*$, $i_{\beta pq\perp}^*$ can be derived (21)(22).

$$i_{\alpha pq\perp}^* = \frac{2}{3} \left(\frac{u_{g\alpha}^+ + k_p u_{g\alpha}^-}{|u_{g\alpha}^+|^2 + k_p |u_{g\alpha}^-|^2} P_{avg} + \frac{u_{g\beta}^+ + k_q u_{g\beta}^-}{|u_{g\beta}^+|^2 + k_q |u_{g\beta}^-|^2} q_{\perp avg}^* \right) \quad (21)$$

$$i_{\beta pq\perp}^* = \frac{2}{3} \left(\frac{u_{g\beta}^+ + k_p u_{g\beta}^-}{|u_{g\beta}^+|^2 + k_p |u_{g\beta}^-|^2} P_{avg} - \frac{u_{g\alpha}^+ + k_q u_{g\alpha}^-}{|u_{g\alpha}^+|^2 + k_q |u_{g\alpha}^-|^2} q_{\perp avg}^* \right) \quad (22)$$

“+” and “-” denote positive and negative sequence components, and k_p , k_q are the factors responsible for the desired targets.

Fig. 2 presents both ways of reference current calculation – (16)-(18) and (21)-(22) – which provide similar results, which means similar waveforms of reference current components in the $\alpha\beta$ frame in both steady states and transient (Fig. 2b). To obtain constant p power in the inverter mode, the $i_{\alpha 2}^*$, $i_{\beta 2}^*$ (18)(19) are applied in the time period from 0.5 to 0.6, and similar results are obtained using $k_p=1$ and $k_q=-1$ in (21)(22). In the rectifier mode in the time period from 0.6 to 0.7, $i_{\alpha 1}^*$, $i_{\beta 1}^*$ (16)(17) are used providing constant virtual torque T_v and similar results are obtained using $k_p=-1$ and $k_q=1$ in (21)(22). Although it can be seen that management of k_p and k_q factors can provide results similar to the proposed method, the automatic change procedure (criteria) of these factors (so the targets) has not been proposed in [17]. The difference between the average values of actual power components and virtual torque components scaled by pulsation are close to the reference (Fig. 2cd), and the error is on a negligible level.

Finally, the reference power and torque components are provided by outer controllers and small steady state error in the inner loop is compensated for.

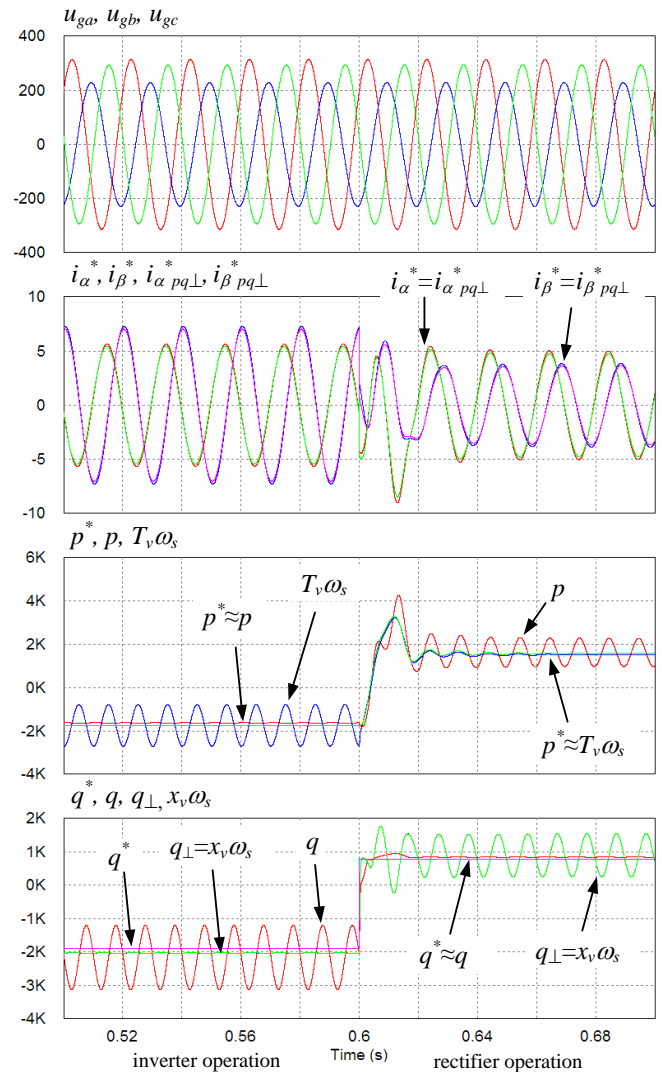


Fig. 2. Simulation results presenting unbalanced grid voltage u_{ga} , u_{gb} , u_{gc} , reference currents obtained with the proposed equations $i_{\alpha 1}^*$, $i_{\beta 1}^*$ before 0.6s, and $i_{\alpha 2}^*$, $i_{\beta 2}^*$ after 0.6s), and with the equations from [17] $i_{\alpha pq\perp}^*$, $i_{\beta pq\perp}^*$ (21)(22), reference T_v^* and actual T_v virtual torque components scaled by ω_s , and the p component of power, and reference q^* , actual q , orthogonal q_{\perp} component of power, and x_v component of virtual torque scaled by ω_s .

C. Calculation of fundamental harmonics grid voltage and virtual flux $\alpha\beta$ components

Components of the voltage vector $u_{g\alpha}$, $u_{g\beta}$ and virtual flux vector $\psi_{g\alpha}$, $\psi_{g\beta}$ can be obtained with several methods. Recently, the most popular ones are second-order generalized integrator structures [17][19] used for calculation of direct and quadrature components of oscillated signals. For flux calculation components, the quadrature component from the SOGI structure must be scaled by the first harmonics pulsation ω_s^{-1} to obtain adequate gain of this output of the SOGI filter. It has been found that the transfer functions of the SOGI filters

represent the second-order low pass filter and the second-order band pass filter. Although the low pass filter gain for frequencies higher than cut-off is low enough to reduce higher frequencies like the 5th and 7th harmonics to a negligible level, the band pass filter responsible for direct component calculation has a significantly higher gain for higher frequencies and cannot eliminate them satisfactorily when they have a high content in the original signal. Therefore, another structure is used to eliminate high frequency components from the measured signals of voltage vector components and calculated virtual flux vector components.

Firstly, the transformation from abc to $\alpha\beta$ coordinates is made. Next, the second-order low pass filters $G_{\psi\alpha_LPF}$, $G_{\psi\beta_LPF}$ ($f_{cutoff}=50\text{Hz}$, damping factor 0.5, gain ω_s^{-1}) are used for calculation of virtual flux components $\psi_{g\alpha}$, $\psi_{g\beta}$. This is to obtain the same dynamic properties of a low pass filter like in the classic SOGI structure. Secondly, second-order high pass filters $G_{u\alpha_HPF}$, $G_{u\beta_HPF}$ ($f_{cutoff}=50\text{Hz}$, damping factor 0.5, gain ω_s) are used for calculation of fundamental frequency components of the grid voltage $u_{g\alpha}$, $u_{g\beta}$. A scheme of grid voltage and virtual flux fundamental components calculation is shown in Fig. 3a, whereas an equivalent diagram is shown in Fig. 3b.

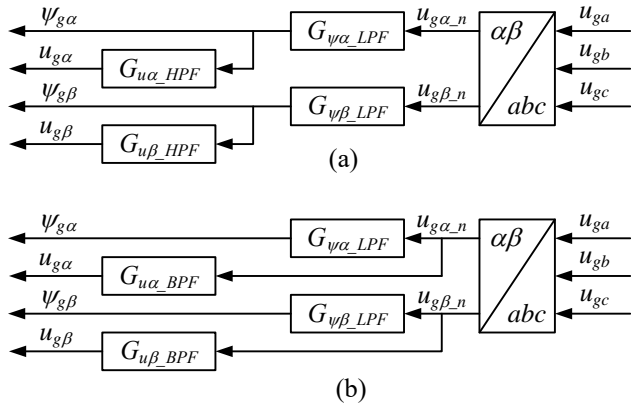


Fig. 3. Scheme of the virtual flux and grid voltage fundamental (50Hz) components calculation method (a), and its equivalent diagram (b).

The used filters have the following transfer functions:

$$G_{\psi\alpha_LPF}(s) = G_{\psi\beta_LPF}(s) = \omega_s^{-1} \frac{\omega_s^2}{s^2 + \omega_s s + \omega_s^2} = \frac{314.16}{s^2 + 314.16s + 314.16^2} \quad (23)$$

$$G_{u\alpha_HPF}(s) = G_{u\beta_HPF}(s) = \omega_s \frac{s^2}{s^2 + \omega_s s + \omega_s^2} = \frac{314.16s^2}{s^2 + 314.16s + 314.16^2} \quad (24)$$

Finally, the u_g to u_{g_n} transfer function of the filters composed with LPF and HPF, can be represented by an equivalent fourth-order band pass filter $G_{u\alpha_BPF}$, $G_{u\beta_BPF}$. and an equivalent u_g to u_{g_n} transfer function takes the form

$$G_{u\alpha_BPF}(s) = G_{u\beta_BPF}(s) = \frac{\omega_s^2 s^2}{(s^2 + \omega_s s + \omega_s^2)^2} = \frac{(314.16s)^2}{(s^2 + 314.16s + 314.16^2)^2} \quad (25)$$

This method reduces the error caused by initial conditions of the integral during virtual flux calculation with the classic method and assures 90 degrees phase shift between respective fundamental components of voltage and flux vectors ($u_{g\alpha}$ –

$\psi_{g\alpha}$, $u_{g\beta}$ – $\psi_{g\beta}$) under fixed frequency. Moreover, it damps the high harmonics components in the signals used for power components calculation more effectively than other methods. Therefore, it is used for the reference current vector components calculation in the method presented in this paper.

Fig. 4 presents the Bode plots of gain and phase characteristics obtained with SOGI filters and the filters used in the paper. It can be seen that a low-pass filter used for flux component calculation has exactly the same gain and phase characteristics as the low-pass filter obtained from SOGI ($|G_{\psi\alpha_LPF}| = |G_{\psi\alpha_SOGI}|$, $\Phi_{\psi\alpha_LPF} = \Phi_{\psi\alpha_SOGI}$), whereas the obtained fourth-order band-pass filter has a lower gain $|G_{u\alpha_BPF}|$ for higher frequencies than the gain $|G_{u\alpha_SOGI}|$ of the second-order band-pass filter obtained from SOGI, whereas both have the same zero phase shift for central frequency 50Hz ($\Phi_{u\alpha_LPF}|^{50\text{Hz}} = \Phi_{u\alpha_SOGI}|^{50\text{Hz}} = 0$).

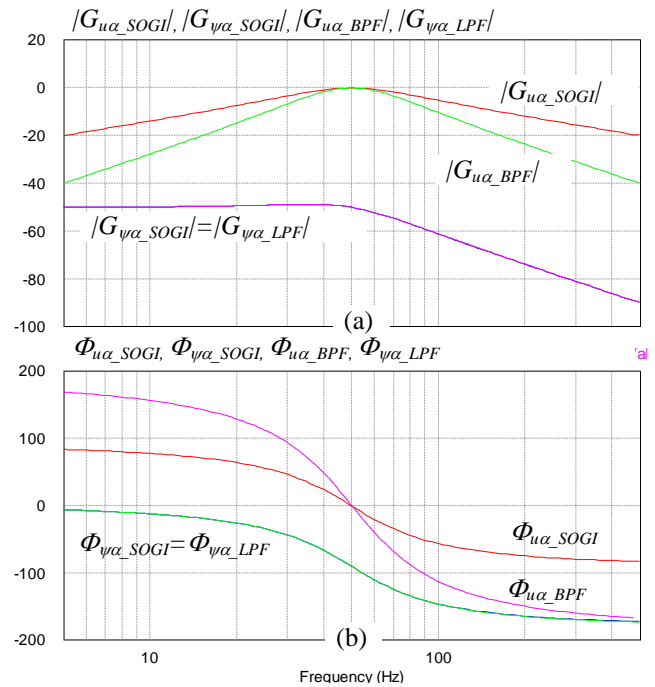


Fig. 4. Bode plots of the SOGI filters and the filters used in the paper for first harmonics grid voltage and virtual flux components calculation, a) gain characteristics of filters in dB, b) phase characteristics of filters in degrees.

Fig. 5 presents the response of SOGI filters and the used filters on the initial step of grid voltage α component distorted by 10% of 5th harmonics. According to the characteristics from Fig. 4, the response of filters for virtual flux (ψ_{α_SOGI} , ψ_{α_LPF}) is the same for both types of structures. The response of an equivalent band-pass filter for the first harmonics of grid voltage (u_{α_BPF}) is slightly slower than the SOGI filter (u_{α_SOGI}), but contains less 5th harmonics in the steady state.

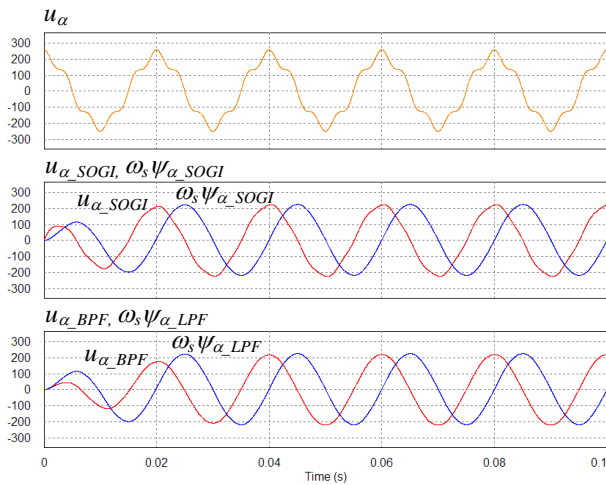


Fig. 5. Simulation results presenting original signal of distorted grid voltage u_α component, first harmonic of the voltage and virtual flux scaled by pulsation calculated by SOGI, first harmonic of the voltage and virtual flux scaled by pulsation calculated with low pass and band pass filters.

III. REFERENCE TARGETS SELECTION

A. Reference targets for inverter and rectifier operation

The current asymmetry opposite to voltage asymmetry in the inverter mode is shown in Fig. 6 in the time period from 0.4s to 0.6s. In the inverter operation mode it may decrease the grid voltage asymmetry factor a_{fu} in the point of common coupling PCC. The current asymmetry corresponding to the voltage asymmetry in the rectifier mode is shown in Fig. 6 in the time period from 0.6s to 0.8s. It does not deepen voltage asymmetry during rectifier operation and the voltage asymmetry factor is the same as during initial state with zero current operation. Influence of the active and reactive current on the grid voltage depends on the grid impedance character. For resistive character, the voltage in PCC may change depending on the active current, whereas for reactive character, the voltage changes depending on the reactive current. Fig. 6 shows the case in which the values of grid resistance and reactance are the same ($R_g=2\Omega$, $X_{Lg}=2\Omega$), but in general it is not representative. However, in most cases, power converters are connected to lines with unidentified grid impedance parameters, which additionally may vary depending on the change of impedance of local load supplied from the same grid.

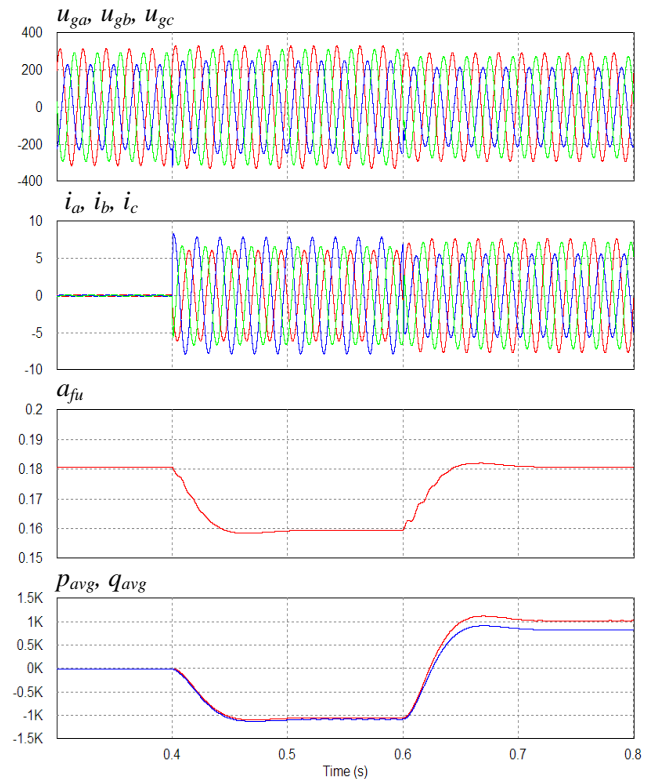


Fig. 6. Simulation results presenting unbalanced grid voltage u_{ga} , u_{gb} , u_{gc} in PCC, unbalanced converter current i_a , i_b , i_c , grid voltage asymmetry factor a_{fu} , average values of pq components of instantaneous power, in the inverter (0.4s-0.6s) and rectifier (0.6s-0.8s) operation, showing the cases of current imbalance beneficial for the power grid.

B. Reference target change depending on the operation mode

In some cases it is difficult to decide what type of current asymmetry will be more beneficial – compatible with grid voltage asymmetry, or opposite. This is because the negative reactive power and the positive active power (rectifier operation with capacitive character of reactive power) may have opposite influence on voltage balancing, when the grid impedance contains both resistance and reactance of a comparable value. The same is in the case of positive reactive power and negative active power (inverter operation with inductive character of reactive power). Fig. 7 presents the inverter operation with different targets of power/current. It can be seen that the influence of active power on voltage asymmetry is compensated for by the influence of reactive power, and the grid voltage asymmetry factor a_{fu} remains almost unchanged. Thus, the only reasonable target in this case is to keep sinusoidal balanced current. In such case the asymmetry factor almost does not change, but the same rms values of currents in each phase cause the smallest total power losses in semiconductors and filter inductors.

When the p and q components have the same sign, it does not matter which target is chosen. For the inverter operation, the negative p and q components of instantaneous power have the same influence on grid voltage asymmetry when the

impedance is simultaneously of inductive and resistive character. As it is shown in Fig. 8, the most desirable target in this case is to keep the current with opposite asymmetry to the asymmetry of grid voltage. This way, the grid voltage asymmetry factor a_{fu} is reduced visibly. Higher symmetrization of the grid voltage is possible, but it requires large power individual source, or many converters operating in the same grid with total power comparable with the grid power.

Taking into consideration that the target can be changed according to the operation mode, it is proposed to introduce a weighting factor a responsible for current balancing when the p and q components of instantaneous power have the opposite sign. This way, the equations (26)(27) are introduced.

$$i_{\alpha}^* = \frac{1}{2} \left((1 + a) i_{\alpha 1}^* + (1 - a) i_{\alpha 2}^* \right) \quad (26)$$

$$i_{\beta}^* = \frac{1}{2} \left((1 + a) i_{\beta 1}^* + (1 - a) i_{\beta 2}^* \right) \quad (27)$$

Although there exist methods of grid impedance identification, most grid power converters are connected to lines with unidentified impedance. Thus, a compromise is selected as a circular hodograph equaling the voltage drop on the line impedance, when the p and q components of instantaneous power have opposite signs (Fig. 10).

Then, the asymmetry weighting factor a equals 0. Depending on the power angle calculated by (28)

$$\phi_p^* = tg^{-1} \left(\frac{q^*}{p^*} \right) \quad (28)$$

factor a is chosen depending on the function shown in Fig. 9.

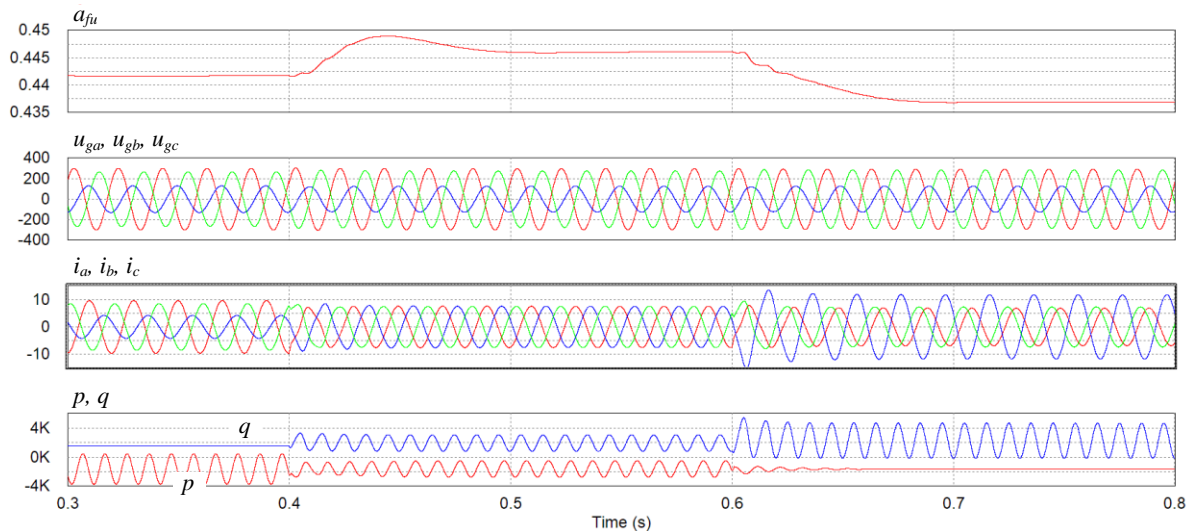


Fig. 7. Simulation results showing the influence of different current asymmetry on the grid voltage asymmetry factor a_{fu} for the positive p component of power (inverter operation) and the negative q component of power (capacitive reactive power).

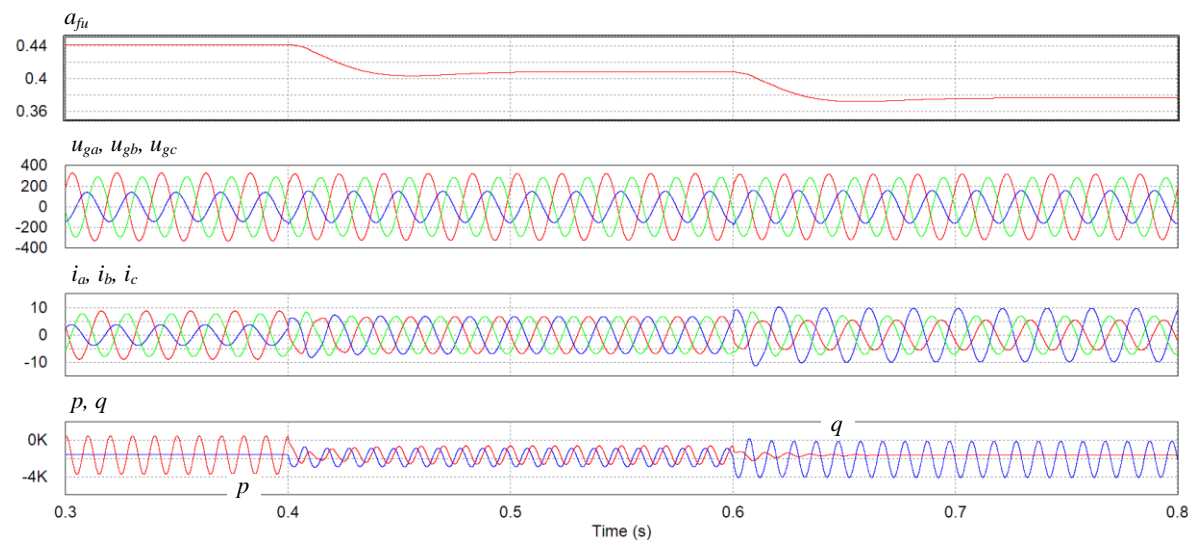


Fig. 8. Simulation results showing the influence of different current asymmetry on the grid voltage asymmetry factor a_{fu} for the negative p component of power (inverter operation) and the negative q component of power (capacitive reactive power).

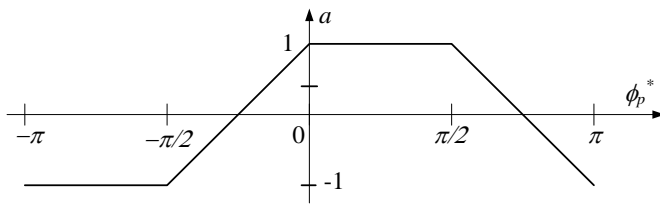


Fig. 9. Reference current asymmetry factor a as a function of power angle ϕ_p^* .

Weighting factor a described by (29)

$$a(\phi_p^*) = \begin{cases} -1, & -\pi < \phi_p^* < -\frac{\pi}{2} \\ \frac{4}{\pi}\phi_p^* + 1, & -\frac{\pi}{2} < \phi_p^* < 0 \\ 1, & 0 < \phi_p^* < \frac{\pi}{2} \\ -\frac{4}{\pi}\phi_p^* + 3, & \frac{\pi}{2} < \phi_p^* < \pi \end{cases} \quad (29)$$

according to the Fig. 9 allows to obtain the current asymmetry in a wide range (from grid voltage asymmetry level to full symmetry), depending on the power angle. A comp view of the current vector asymmetry as exemplary hodographs depending on the power angle is presented in Fig. 10.

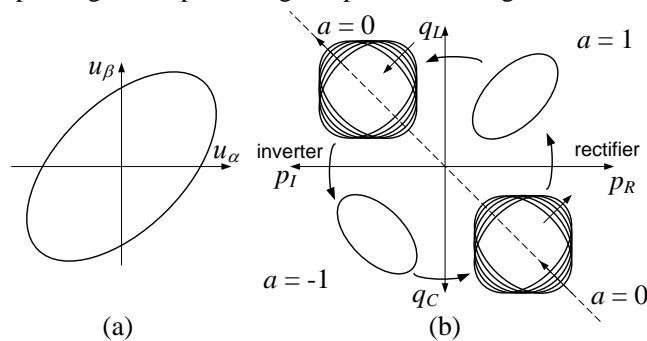


Fig. 10. Assignment of the inverter and rectifier modes regions, a) unbalanced grid voltage vector exemplary hodograph, and b) visualization of current vector hodographs in each region (I quadrant – ($a = 1$), II quadrant – ($-1 < a < 1$); $a = 0$ for $\phi_p^* = 135^\circ$), III quadrant – ($a = -1$), IV quadrant – ($-1 < a < 1$); $a = 0$ for $\phi_p^* = -45^\circ$).

C. Reference targets depending on current limitation level

Although the constant p (simultaneously constant x_v) or constant q (simultaneously constant T_v) targets are beneficial for the grid in separate cases (inverter/rectifier) respectively, the possible power, which can be transferred when phase current limitation is kept, is lower than for symmetrical current. Thus, the method of current progressive balancing is proposed to increase the power transfer in both modes if necessary. Current vector instantaneous length limitation can be used only in the case of balanced sinusoidal current. In the other targets which cause asymmetrical current, the current vector length is no longer constant. The circle representing maximum vector length cuts the elliptic hodograph when the actual current vector length reaches instantaneously the maximum value. In this case the hodograph looks like in Fig. 11a, and it means that the phase currents will be distorted.

The second method of current limitation is based on cutting the vector length by a hexagon. This corresponds to the limitation of the instantaneous value of phase current in each phase respectively. Fig. 11b shows the current hodographs for the described limitation method, which do not provide sinusoidal phase currents at this state, but produce the flat-top sine wave exceeding the limited rms at least in one phase.

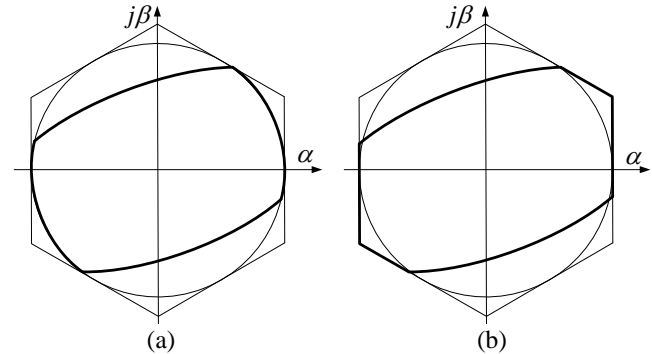


Fig. 11. Hodographs of converter current, a) when the vector length is limited by a circle representing the maximum vector length, b) when the instantaneous vector length is limited by a hexagon representing maximum instantaneous value of the phase currents.

The maximum elliptic hodograph of unbalanced current keeping the grid voltage asymmetry, which can be inscribed inside the circle representing maximum symmetrical current, is drawn with a bold line in Fig. 12a. Depending on the ellipse major axis angle, the phase current may be equal to the maximum phase current in at least one phase. When the orientation of the major axis does not overlap with one of the phase axes, all phase currents are lower than the maximum, because the ellipse does not touch the hexagon. The power demand may increase the value of the current and the hodograph may be changed to a circular form, allowing full balancing of current as the final stage. This way the current is less useful for the grid, but it increases the power, which may be critical especially in the rectifier mode not to cause DC voltage drop.

The phase current true limitation requires a number of calculations [15] and a powerful controller when the reference current is assigned by determination of the ellipse orientation in relation to the phase axes, whereas it has to be noted that current limitation is only one of several procedures taken into account in the control method. The phase rms current true limitation allows to obtain a larger hodograph (Fig. 12b) than the one from Fig. 12a, which means higher power when current asymmetry is kept at the level of grid voltage asymmetry. However, the power is still lower than possible maximum power, which can be transferred by symmetrical current. Thus, the progressive balancing procedure can be applied to the current limitation method.

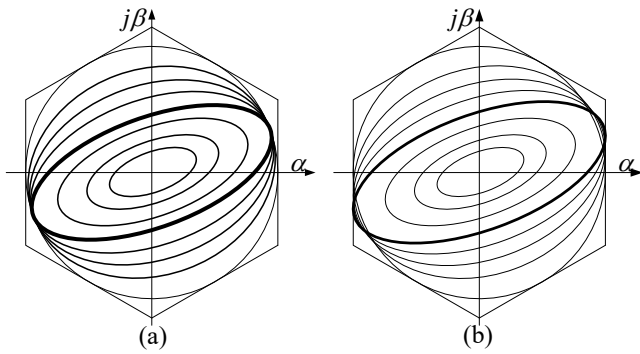


Fig. 12. Possible hodographs of converter current during progressive balancing when a) the elliptic hodograph does not exceed the maximum circle, b) the elliptic hodograph does not exceed the hexagon.

The last current limitation way has been implemented to obtain the results described in the paper. The algorithm of progressive current balancing will be described here. The goal in the rectifier mode is not to deepen the grid voltage asymmetry for lower power demand and to obtain maximum possible power at a given grid voltage asymmetry for higher power demand. In the inverter mode the goal is to decrease the

grid voltage asymmetry for lower produced power and to obtain maximum possible power for higher power production. The proposed method of current balancing is to calculate the weighted average of the reference current i_{α}^* , i_{β}^* (26)(27) based on (16)-(19), whereas the reference current asymmetry is based on the factor ξ depending on the current limitation.

$$i_{\alpha}^* = \frac{1}{2} \left((1 + \xi a) i_{\alpha 1}^* + (1 - \xi a) i_{\alpha 2}^* \right) \quad (30)$$

$$i_{\beta}^* = \frac{1}{2} \left((1 + \xi a) i_{\beta 1}^* + (1 - \xi a) i_{\beta 2}^* \right) \quad (31)$$

When at least one of the phase current exceeds the limit, the weighting factor ξ is decreased from 1 to 0. Finally, symmetrical current can be obtained as the average value of reference current for constant virtual torque T_v and constant p targets, respectively. Progressive balancing providing asymmetrical to symmetrical current transient for rectifier and inverter operation with zeroed average value of the q component of power is shown in Fig. 13.

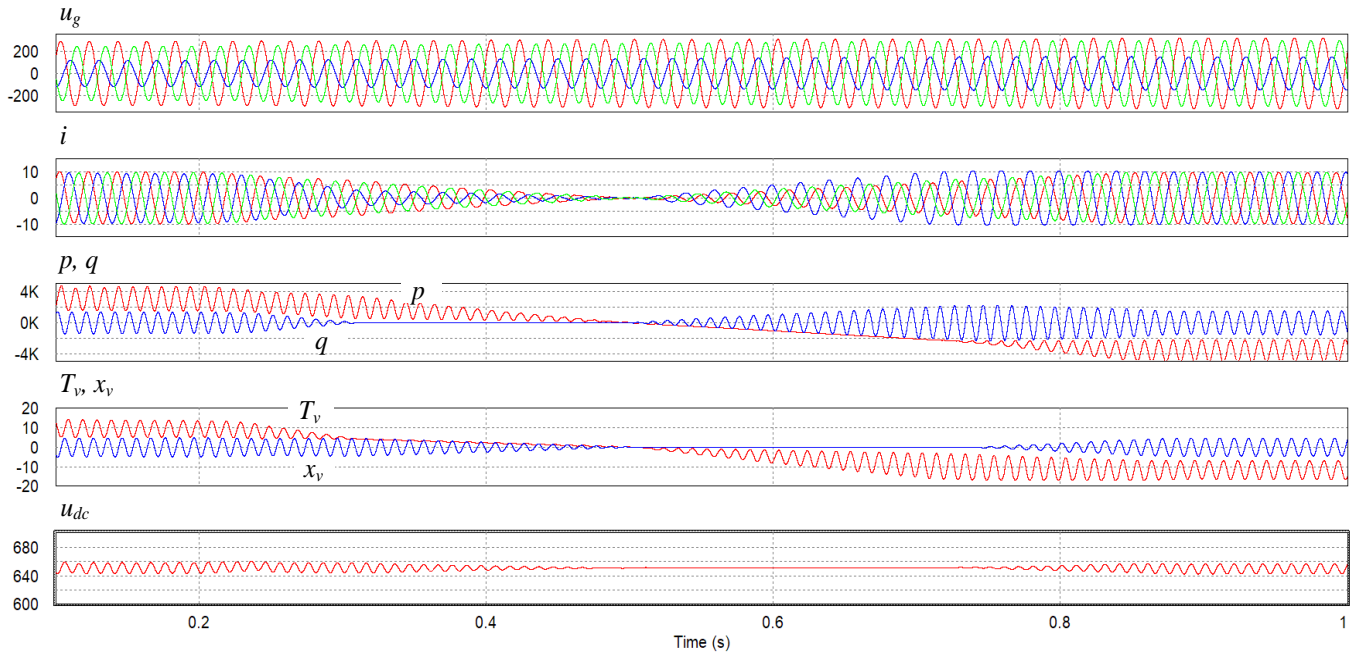


Fig. 13. Simulation results presenting targets change from symmetrical current through the corresponding asymmetry of current in the rectifier mode, next through the opposite current asymmetry to the symmetrical current in the inverter mode at zeroed average q component of instantaneous power.

D. Control structure of grid converter operating as an inverter and a rectifier at unbalanced grid voltage

The whole proposed control structure is presented in Fig. 14 – the reference current components calculation for both targets of current asymmetry (constant p component recommended for inverter operation, and constant q component recommended for rectifier operation), the way of calculation of resultant current with reduced asymmetry or fully balanced depending on the factor ξ responsible for the current

limitation, and the factor a related to the operation mode and power angle. The way of reference current limitation and phase current limitation factor ξ assignment is based on the sinusoidal phase current rms value calculated separately for each phase. This part of control firstly tries to balance the current by decrease of weighting factor ξ from 0 to 1, and next after full balancing, if the value of reference balanced current vector length still exceeds the maximum value, the current components are scaled by the factor k_{limit} (32), which equals one for the reference current smaller than the limit, and less

B. Progressive balancing caused by current limitation

Fig. 15 shows the case of progressive balancing implemented in the pure rectifier mode with the zero reference q component of power. The test is recorded from the point of very low current increased proportionally in each phase until one of the phase currents reaches the maximum value. Then progressive balancing of current is done to increase power transferred from the grid to the DC link. The grid voltage asymmetry type places the major axis of grid voltage elliptic hodograph almost along the c phase axis. Therefore, the maximum current vector length equals the amplitude of the maximum phase current. This is why only the minor axis of the current elliptic hodograph is progressively increased to obtain the balanced current and the major axis is not changed after reaching the phase current limitation.

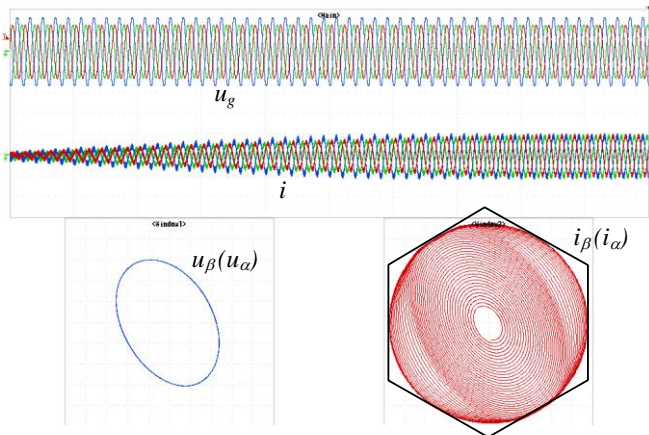


Fig. 15. Unbalanced grid voltage u_g and converter current i , and voltage and current hodographs during current progressive balancing in the rectifier mode.

Fig. 16 presents the case of progressive balancing implemented for inverter operation. The starting point of registration is a very low current increased proportionally in each phase until the phase current reaches the maximum value. In this point, the elliptic hodograph exceeds the circular hodograph of maximum symmetrical current, but does not exceed the hexagon, so the maximum phase current is not exceeded. From this point, the minor axis is increased to enlarge the transferred power, whereas the major axis is slightly decreased not to exceed the hexagon lines. In both tests from Fig. 15 and 16, the voltage hodograph is registered with 50V/div in each axis, whereas the current vector hodograph is normalized, to make the hodographs as readable as possible.

C. Progressive balancing depending on the operation mode

Fig. 17 presents the progressive target change depending on the operation mode described in section 3.2. The test has been made in the way that the DC voltage is stabilized from an external source, the reference apparent power has been set constant, and the power angle ϕ_p^* has been changed from $-\pi$ to π . This way both pure inverter and rectifier operation modes

have been obtained, as well as intermediary states, in which it is difficult to define which target should be realized, so symmetrical current is referenced.

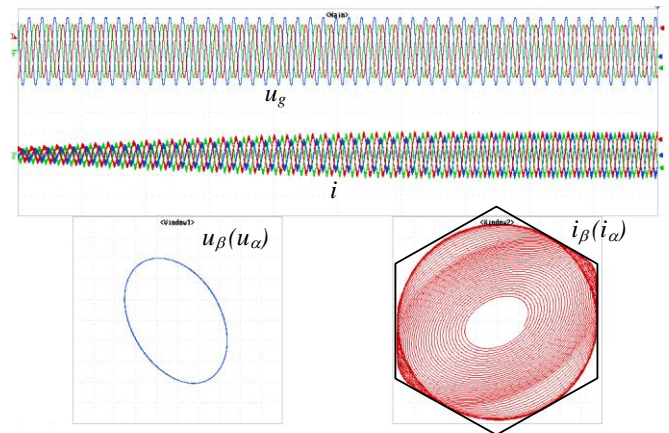


Fig. 16. Unbalanced grid voltage u_g and converter current i , and voltage and current hodographs during current progressive balancing in the inverter mode.

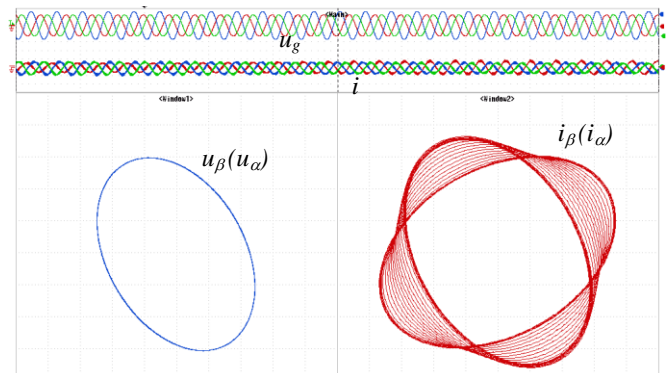


Fig. 17. Unbalanced grid voltage u_g and converter current i , and voltage and current hodographs during current progressive balancing depending on the operation mode and power angle.

D. Transient states of power components step change

Fig. 18 presents transients caused by step loading by i_{dc} current causing change of the reference converter current for the rectifier mode. For this target the reference current is calculated on the basis of constant reference virtual torque and zero reference reactive power. There are visible oscillations on the DC voltage. Fig. 18a presents step loading of the rectifier by load power that does not cause current limitation, so current asymmetry corresponds to voltage asymmetry. Fig. 18b presents step unloading to zero, and the initial load power causes current limitation, so the current is symmetrical.

Fig. 19 presents the case of inverter operation starting from zero i_{dc} source current and transient caused by the i_{dc} change. Fig. 19a presents the case in which the DC source power does not cause current limitation, so current asymmetry is opposite to voltage asymmetry. Fig. 19b presents the case in which the DC source power causes current limitation, and the current is balanced. Higher energy transfer from the DC source causes an increase of the DC voltage over reference value due to the converter current limitation, and to avoid DC overvoltage, an

additional maximum DC voltage controller was implemented in the DC source to reduce the DC source power and to obtain safe steady-state operation. In practice, this means limitation of power produced by a source like PV or a wind turbine connected to the DC link, when the converter current constraint is obtained.

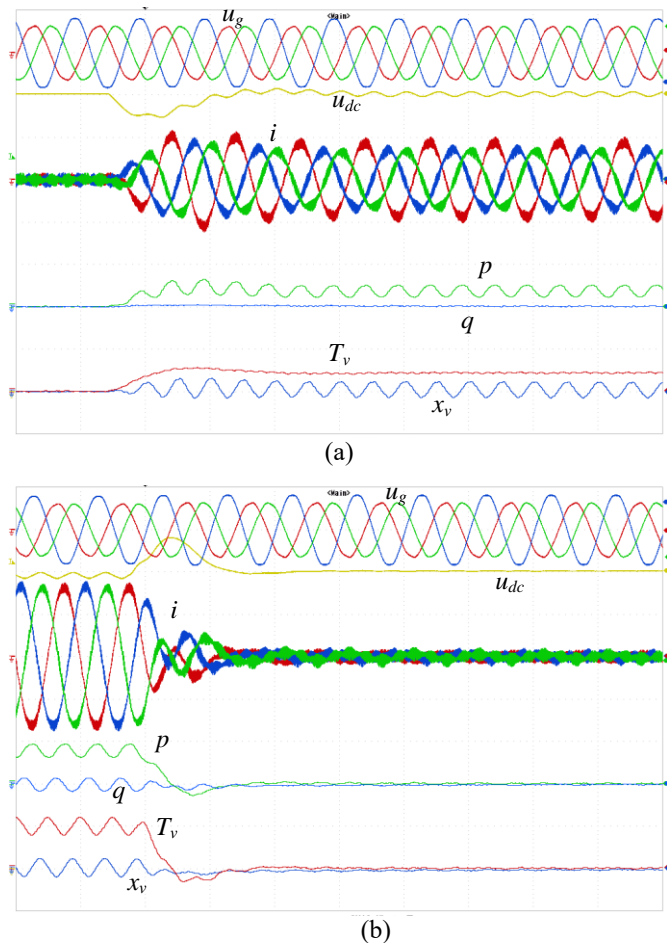


Fig. 18. Unbalanced grid voltage u_g , DC voltage u_{dc} , converter current i , pq power components, and virtual torque components T_v , x_v during the rectifier mode, a) dynamic loading not causing phase current limitation, b) dynamic unloading from the level causing full balancing of current to zero.

Fig. 20 presents the case of the p and q power components change (transfer of operating points between neighboring quadrants shown in Fig. 10b). In each quadrant the average reference p and q power components have equal absolute values and the same or opposite signs. Initially, in Fig. 20a, the transient from the first to second quadrant and back through the change of active power is shown. For the inductive q component of power, converter current has asymmetry corresponding to the voltage asymmetry for rectifier operation and it is symmetrical for inverter operation. Fig. 20b presents transients from the second to third quadrant and back. For inverter operation the converter current is symmetrical for the inductive q component of power and has asymmetry opposite to the grid voltage asymmetry for the

capacitive q component of power. Fig. 20c presents the transient from the third to fourth quadrant and back. For the capacitive q component of power the converter current has asymmetry opposite to voltage asymmetry and it is symmetrical for rectifier operation. Fig. 20d presents the transient from the fourth to first quadrant and back. For rectifier operation the converter current is symmetrical for the capacitive q component of power and has asymmetry opposite to voltage asymmetry for the inductive q component of power. In Fig. 20a and Fig. 20c every step of the p component of power (changes from inverter to rectifier operation and opposite) causes short time DC voltage dips or swells. In this experiment, the DC voltage was controlled by the second converter connected with the DC bus, simulating DC load or source depending on the sign of the p component of power.

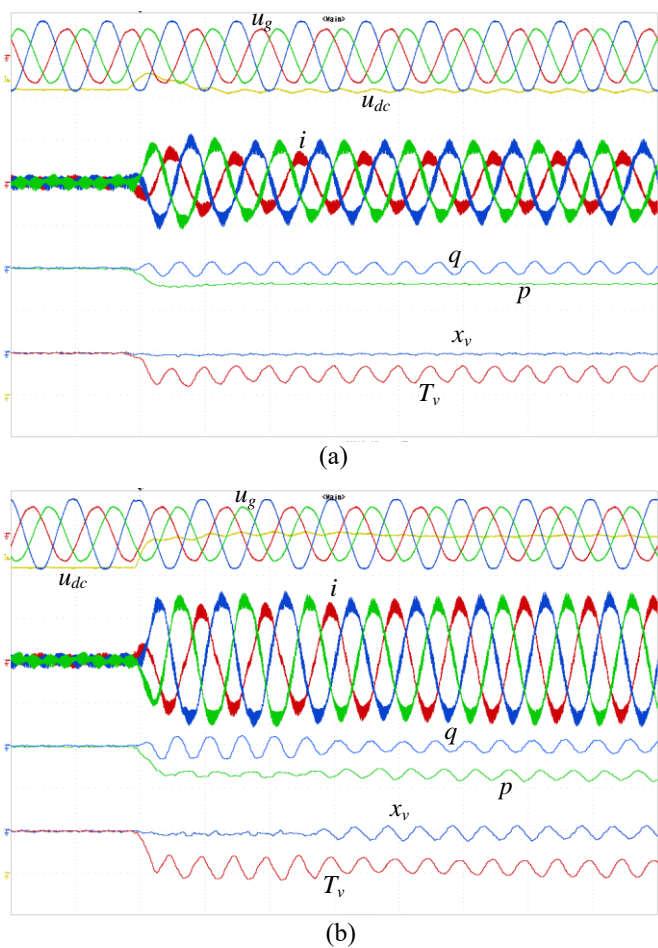


Fig. 19. Unbalanced grid voltage u_g , DC voltage u_{dc} , converter current i , pq power components, and virtual torque components T_v , x_v during inverter mode, a) dynamic change of the DC source power not causing phase current limitation, b) dynamic change of the load power causing full balancing of current.

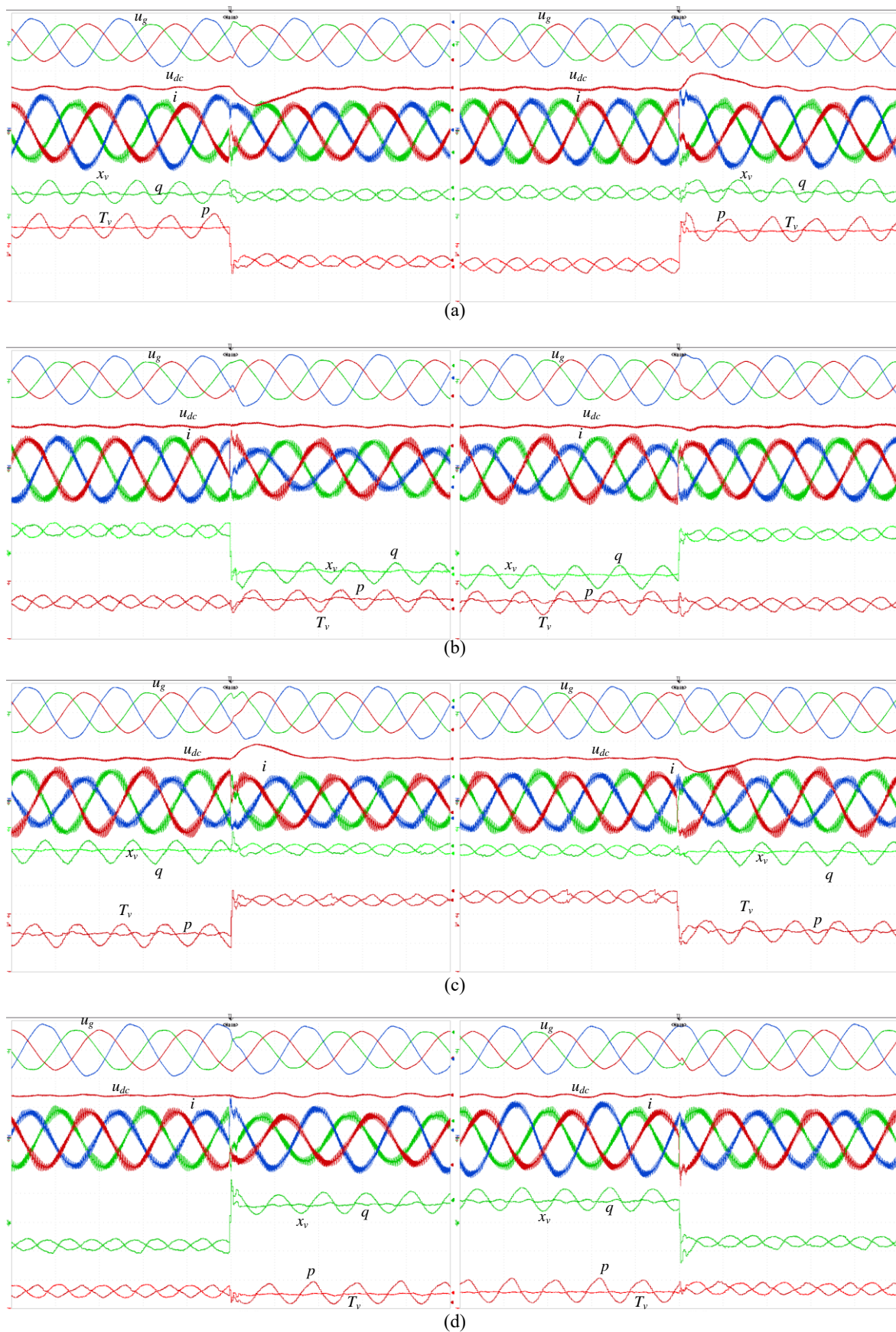


Fig. 20. Unbalanced grid voltage u_g , DC voltage u_{dc} , converter current i , p q power components, and virtual torque components T_v , x_v during transients steps of reference power, a) transfer from first to second quadrant and back, b) transfer from second to third quadrant and back, c) transient from third to fourth quadrant and back, d) transient from fourth to third quadrant and back.

E. Converter operation under simultaneous grid voltage imbalance and harmonics distortions

The method used for reference current calculation provides good filtration of harmonics in the grid voltage and grid virtual flux. Therefore, the obtained current, despite simultaneous grid voltage asymmetry and harmonics, can still be sinusoidal with the desired asymmetry. Inverter operation with simultaneous grid voltage harmonics and imbalance is shown in Fig. 21. The current does not contain harmonics, whereas it is asymmetrical with asymmetry corresponding to the voltage asymmetry in the case of rectifier operation (Fig. 21a), and with asymmetry opposite to the grid voltage asymmetry in inverter operation (Fig. 21b). As the pq power components and T_v, x_v instantaneous virtual torque components are here calculated with the use of actual non-filtered voltage and virtual flux $\alpha\beta$ components, the oscillations of these variables are not sinusoidal, but they contain 300Hz oscillations caused by dominating 5th and 7th harmonics produced by nonlinear load (three-phase six pulse diode rectifier) connected in parallel to the lines.

F. Transient response to the grid voltage asymmetrical dip

Fig. 22 presents the case of grid voltage asymmetry transient caused by a short-time two-phase line-to-line significant overload during inverter operation of the grid converter. The initial current is symmetrical due to voltage balancing, whereas during transient the current asymmetry becomes opposite to the voltage asymmetry adequate for the inverter operation. The transient of the current waveform is quite short i.e. less than two periods of the grid voltage. Transients are caused by introduction of filters used for determination of fundamental harmonics of grid voltage and grid virtual flux.

The whole control system includes only three nonlinear functions that take a number of computational cycles in the DSP microcontroller. The first one is a division in eq. (16)(17) and (18)(19). Once calculated term:

$$\frac{1}{\psi_{g\alpha} u_{g\beta} - \psi_{g\beta} u_{g\alpha}} \quad (33)$$

can be used in multiplication operation in all these equations (16)-(19), that take less cycles than four times used division. The second is the equation calculating reference current vector length $|i^*|$ for limitation when balanced reference current exceeds the limit. The third one is a function used for balanced current limitation factor k_{limit} calculation (32). These nonlinear functions are division (twice) and square root. In the control system there are avoided calculation of \sin , \cos , tg , tg^{-1} , or other trigonometric functions, which take a lot of computational cycles. In the experiment, as the control unit a DSP controller build with TMS320F28335 was used. The controller is in the family widely used in industrial applications in the field of power electronics and drives. All

other nonlinear functions are not troublesome in calculations (e.g. saturation blocks are computed using comparators). All filters are the natural structures for DSP controllers, which are calculated fast in a few computational cycles. This is why the control can easily be applied in industrial version of grid converter.

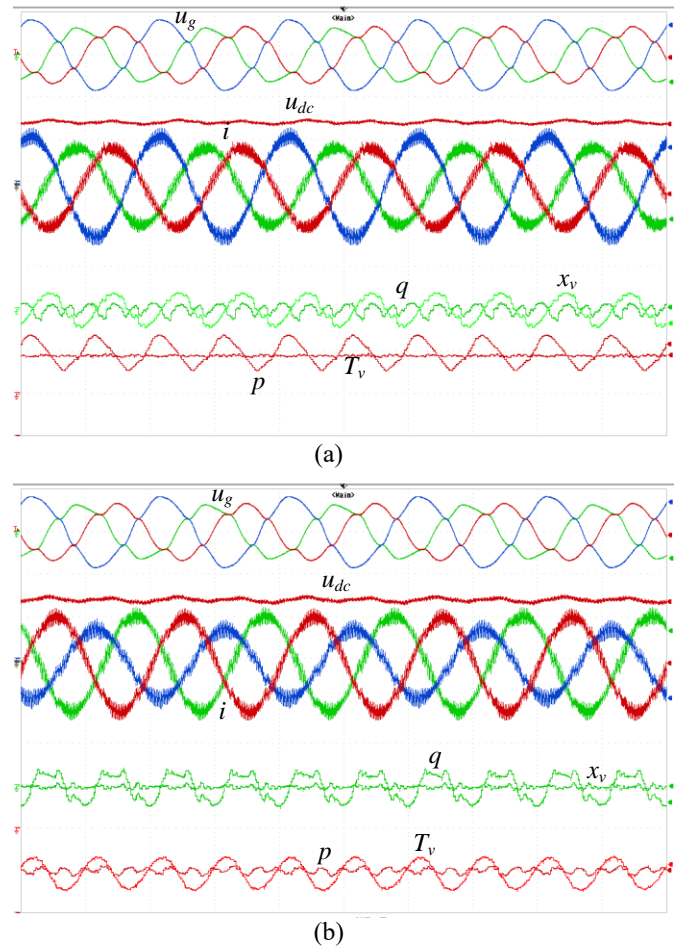


Fig. 21. Unbalanced and harmonics distorted grid voltage u_g , DC voltage u_{dc} , converter current i , pq power components, and virtual torque components T_v , x_v during a) the rectifier mode, and b) the inverter mode, at zeroed reference q component of instantaneous power.

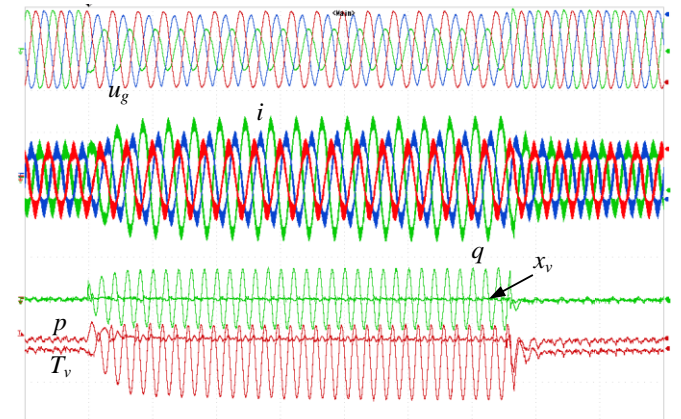


Fig. 22. Grid voltage u_g , DC voltage u_{dc} , converter current i , pq power components, and virtual torque components T_v , x_v during the inverter mode at grid voltage imbalance transients.

V. CONCLUSION

The paper presents the concept and exemplary control of grid converter current progressive balancing during different targets such as constant p , constant q or symmetrical current. The innovative part is to use variables which can be easily calculated and some of which are constant in separate targets of asymmetrical current respectively. The reference current calculated on the basis of two opposite targets (constant p , and constant T_v), is a weighted value of currents calculated for these two targets, and the weights depend on both – the operation mode and phase current constraints. The method of phase current limitation is based on phase current signals and may be applied to four-wire systems as well. The proposed control method is adequate for both rectifier and inverter modes and for reactive power referenced in a wide range. It also covers the whole range of power angle from $-\pi$ to π . The function of asymmetry weighting factor a (Fig. 9) can be modified in different manners to obtain e.g. higher current asymmetry than asymmetry of grid voltage. However, it requires further study about the influence of the current asymmetry on the grid voltage for different grid impedance character. Possibly, even combination of this function with the algorithm of grid impedance estimation may be applied. However, it will not change the core of proposed the control method.

APPENDIX

List of symbols

u_{ca}, u_{cb}, u_{cc} – converter phase voltage
 i_a, i_b, i_c – converter phase current
 u_{ga}, u_{gb}, u_{gc} – grid phase voltage
 $u_{g\alpha_n}, u_{g\beta_n}$ – natural grid voltage vector components in stationary coordinates without filtration
 $u_{g\alpha}, u_{g\beta}$ – fundamental (50Hz) grid voltage vector components in stationary coordinates obtained by filtration
 $\psi_{g\alpha}, \psi_{g\beta}$ – fundamental (50Hz) grid virtual flux vector components in stationary coordinates
 i_α, i_β – current vector components in stationary coordinates
 $u_{g\alpha}^d, u_{g\beta}^d$ – grid voltage vector components in stationary coordinates delayed by $\pi/2$
 u_{dc} – DC bus voltage
 i_{dc} – DC source/load current
 pq – instantaneous power components by Akagi
 T_v, x_v – instantaneous virtual torque components
 q_\perp – q component of power calculated by dot product of grid voltage vector delayed by $\pi/2$ and converter current vector
 $i_{\alpha 1}^*, i_{\beta 1}^*$ – reference current vector components for constant virtual torque T_v (rectifier operation)
 $i_{\alpha 2}^*, i_{\beta 2}^*$ – reference current vector components for constant p component of power (inverter operation)

$i_{\alpha pq\perp}^*, i_{\beta pq\perp}^*$ – reference current vector components calculated with the use of q_\perp
 a_{fu} – grid voltage asymmetry factor
 a – reference current asymmetry factor depending on the operation mode (in the range from -1 to 1)
 ξ – symmetrization factor depending on the current limitation (in the range from 0 to 1)
 ω_s – synchronous pulsation of the grid voltage
 $|i|$ – current vector instantaneous length
 i_{ref}^{max} – reference limitation of the phase current amplitude
 i_{refavg}^{max} – reference limitation of the phase current average value
 $i_{alimit}^*, i_{blimit}^*, i_{climit}^*$ – reference limited instantaneous phase current
 $i_{aavg}^*, i_{bavg}^*, i_{cavg}^*$ – reference limited average phase current

REFERENCES

- [1] C. T. Rim, N. S. Choi, G. C. Cho, and G. H. Cho, "A complete DC and AC analysis of three-phase controlled-current PWM rectifier using circuit D-Q transformation," *IEEE Trans. Power Electron.*, vol. 9, pp. 390–396, July 1994.
- [2] N. R. Zargari and G. Joos, "Performance investigation of a current-controlled voltage-regulated PWM rectifier in rotating and stationary frames," *Int. Conf. on Industrial Electronics, Control and Instrumentation-IECON'93*, Maui, Hawaii, USA, 1993, pp. 1193–119.
- [3] T. Noguchi, H. Tomiki, S. Kondo, I. Takahashi, "Direct Power Control of PWM converter without power-source voltage sensors.," *IEEE Trans. on Ind. Applications*, vol. 34, no. 3, pp. 473-479, May/June 1998.
- [4] T. Ohnishi, "Three-phase PWM converter/inverter by means of instantaneous active and reactive power control", *Ind. Electron. Conf. -IECON'91*, Kobe, Japan, 1991, pp. 819-824,
- [5] M. Malinowski, M.P. Kazmierkowski, S. Hansen, F. Blaabjerg, G. D. Marques, "Virtual flux based Direct Power Control of three-phase PWM rectifier", *IEEE Trans. Ind. Appl.*, vol. 37, no. 4, pp. 1019-1027, Jul/Aug 2001
- [6] M. Malinowski, M. Jasiński, and M. P. Kazmierkowski, "Simple Direct Power Control of three-Phase PWM Rectifier Using Space-Vector Modulation (DPC-SVM)," *IEEE Trans. Ind. Electronics*, vol. 51, no. 2, pp. 447– 454, April 2004.
- [7] P. Rioual et al., "Regulation of a PWM Rectifier in the Unbalanced Network State", *Power Electron. Spec. Conf. – PESC*, Seattle, USA, 1993, pp. 641-647
- [8] H.S. Kim et al., "Design of Current Controller for Three-Phase PWM Converter with Unbalanced Input Voltage," *IEEE 29th Annual Power Electron. Spec. Conf. –PESC'98*, Fukuoka, Japan, 1993, pp. 503-509
- [9] G. Saccomando, J. Svensson, "Transient operation of grid-connected voltage source converter under unbalanced voltage conditions," *36th IAS Annual Meeting*, vol. 4, Sept. 30, 2001, pp. 2419-2424
- [10] C. Ng, L. Ran and J. Bumby, "Unbalanced Grid Fault Ride-Through Control for a Wind Turbine Inverter," *Industry*

- Applications Conference, 2007. 42nd IAS Annual Meeting*, New Orleans, USA, 2007, pp. 154-164.
- [11] L. Hang and M. Zhang, "Constant power control-based strategy for Vienna-type rectifiers to expand operating area under severe unbalanced grid", *IET Power Electronics*, vol. 7, no. 1, pp. 41-49, January 2014.
- [12] A.V. Stankovic, Ke Chen, "A New Control Method for Input–Output Harmonic Elimination of the PWM Boost-Type Rectifier Under Extreme Unbalanced Operating Conditions," *IEEE Trans. Industrial Electronics*, vol. 56, no. 7, pp. 2420-2430, July 2009
- [13] D. Roiu, R.I. Bojoi, L.R. Limongi, A. Tenconi, "New Stationary Frame Control Scheme for Three-Phase PWM Rectifiers Under Unbalanced Voltage Dips Conditions," *IEEE Tran. Industry Applications*, vol. 46, no. 1, pp. 268-277, Jan.-Feb. 2010
- [14] H.-G. Jeong, U.-M. Choi, and K.-B. Lee, "Control strategies for wind power systems to meet grid code requirements", *Proc. IEEE 37th Annu. Conf. Ind. Electron. Soc.*, 2011, pp. 1250–1255.
- [15] A. Milicua, G. Abad, M.A. Rodriguez Vidal, "Online Reference Limitation Method of Shunt-Connected Converters to the Grid to Avoid Exceeding Voltage and Current Limits Under Unbalanced Operation—Part I: Theory," *IEEE Trans. Energy Conv.*, vol. 30, no. 3, pp. 852-863, Sept. 2015
- [16] Z. Ivanovic, M. Vekic, S. Grabic, and V. Katic, "Control of multilevel converter driving variable speed wind turbine in case of grid disturbances", *Proc. 12th Int. Power Electron. Motion Control Conf.*, 2006, pp. 1569–1573.
- [17] J. A. Suul, "Control of grid integrated voltage source converters under unbalanced conditions" Ph.D. dissertation, Dept. Elect. Power Eng., Norwegian Univ. Sci. Technol., Trondheim, Norway, 2012.
- [18] M. Castilla, J. Miret, A. Camacho, J. Matas, and L. Garcia de Vicuna, "Voltage support control strategies for static synchronous compensators under unbalanced voltage sags," *IEEE Trans. Ind. Electron.*, vol. 61, no. 2, pp. 808–820, Feb. 2014.
- [19] P. Rodriguez, G. Medeiros, A. Luna, M. C. Cavalcanti, and R. Teodorescu, "Safe current injection strategies for a STATCOM under asymmetrical grid faults," *Proc. IEEE Energy Convers. Congr. Expo.*, 2010, pp. 3929–3935.
- [20] A. Camacho, M. Castilla, J. Miret, A. Borrell, and L.G. de Vicuña, "Active and Reactive Power Strategies With Peak Current Limitation for Distributed Generation Inverters During Unbalanced Grid Faults", *IEEE Trans. Ind. Electron.*, vol. 62, no. 3, pp. 1515 – 1525, March 2015
- [21] W. Jiang, Y. Wang, J. Wang, L. Wang, and H. Huang, "Maximizing Instantaneous Active Power Capability for PWM Rectifier Under Unbalanced Grid Voltage Dips Considering the Limitation of Phase Current", *IEEE Trans. Ind. Electron.*, vol. 63, no. 10, pp. 5998-6009, Oct 2016
- [22] F. Wang, J. L. Duarte and M. A. M. Hendrix, "Pliant Active and Reactive Power Control for Grid-Interactive Converters Under Unbalanced Voltage Dips" in *IEEE Transactions on Power Electronics*, vol. 26, no. 5, pp. 1511-1521, May 2011.
- [23] G. Iwanski; T. Luszczuk; M. Szypulski, "Virtual Torque Based Control of Three Phase Rectifier Under Grid Imbalance and Harmonics," *IEEE Transactions on Power Electronics*, vol. 32, no. 9, pp. 6836-6852, Sept. 2017
- [24] L. Xu, and Y. Wang, "Dynamic Modeling and Control of DFIG-based Wind Turbines under Unbalanced Network Conditions," *IEEE Trans. Power Syst.*, vol. 22, no. 1, pp. 314–323, Feb. 2007.



Grzegorz Iwanski received the M.Sc. degree in automation and robotics, and the Ph.D. degree in electrical engineering from Warsaw University of Technology (WUT), Warszawa, Poland, in 2003 and 2005, respectively. Since January 2006 to December 2008 he was a research worker in the Institute of Control and Industrial Electronics of WUT involved in international project within 6th Framework Programme of EU. Since 2009 he has been an Assistant Professor in Institute of Control and Industrial Electronics WUT.

He teaches courses on power electronics, drives and power conversion systems. His research interests include variable and adjustable speed power generation systems, photovoltaic and energy storage systems, automotive power electronics and drives. In 2012/2013 he joined the team of REES UPC, Barcelona –Terrassa, within the framework of scholarship of Polish Minister of Science and Higher Education for investigation of power converters topologies with reduced common-mode component for photovoltaic systems. He is co-author of one monograph, three books chapters and 60 journal and conference papers.